Generative Representation of Aggregate Brain Activity: A Deep Autoencoder Approach for EEG Topoplot Summarization

Tobias Mikha Sulistiyo[1], Karel Octavianus Bachri[2]*
School of Bioscience, Technology, and Innovation,
Atma Jaya Catholic University of Indonesia, Jakarta, Indonesia[1], [2]
tobias.12024002503@student.atmajya.ac.id[1], karel.bachri@atmajaya.ac.id [2]

***Abstract*—Visualizing group-level EEG characteristics is essential for understanding cognitive states, yet traditional pixel-wise averaging often obscures spatial specificity and fails to eliminate baseline artifacts effectively. To address these limitations, this study proposes a Deep Convolutional Autoencoder (CAE) framework to implement Latent Space Aggregation for two-dimensional EEG topography. Unlike standard arithmetic averaging, this method compresses topoplots into a latent feature space to capture structural invariants before reconstructing a representative group-level image. The proposed framework was evaluated using a dataset of adolescents responding to addiction-related terminology, stratified by risk status (Normal vs. At-Risk) and reaction latency (Fast vs. Slow). The generative reconstruction revealed distinct neurocognitive strategies: while Normal subjects exhibited regulated frontal-temporal engagement, At-Risk Fast responders demonstrated global cortical hyper-arousal indicative of impulsivity. Conversely, At-Risk Slow responders displayed posterior-dominant activation (Occipital-Temporal) with diminished frontal control, supporting the Attentional Bias hypothesis. These findings validate the CAE approach as a robust tool for artifact suppression and high-fidelity signal preservation, offering a novel methodological pathway for interpreting complex neural dynamics in addiction research.**

Keywords— Deep Convolutional Autoencoder (CAE), Latent Space Representation, Addiction, Unsupervised Learning, Image Reconstruction.

I. INTRODUCTION

Visualizing EEG signals in two dimensions is one way to represent EEG signals for easier analysis. This technique enables the spatial distribution of electrical activity across the scalp to be mapped onto a two-dimensional image, providing a clearer and more intuitive depiction of the underlying brain dynamics [1], [2]. Using this method helps both clinicians and non-expert users more easily understand EEG activity at a given point in time. In population-based studies, however, the primary challenge does not lie in analyzing individual subjects, but rather in integrating data from multiple participants to obtain a valid and reliable group-level representation [3]. Data aggregation therefore becomes essential for identifying spatial patterns that accurately differentiate conditions within the plotted scalp maps [2].

However, aggregation methods exhibit a fundamental limitation that is often overlooked. The standard approach still relies heavily on computing the pixel-wise arithmetic mean across all images within a dataset. Such averaging procedures can obscure meaningful spatial variations, reduce inter-subject specificity, and potentially distort group-level representations of EEG activity [4]. In many EEG datasets, line-shaped activation patterns tend to be consistently detected as meaningful neural activity. However, when these patterns vary across subjects or trials, the pixel-wise averaging process inevitably incorporates these variations into the final aggregated image. As a result, the computed average may become biased or distorted at specific pixel locations, leading to an inaccurate representation of the underlying neural signal.

Recent progress in deep learning has opened new opportunities to address the limitations of traditional statistical aggregation methods. One approach that has become increasingly popular is the use of Convolutional Autoencoders (CAEs), which have shown strong potential in representing EEG data more effectively than simple pixel averaging [5], [6]. Instead of working directly with raw images, autoencoders learn to compress the input into a latent feature space that captures the most relevant structure of the data.

This latent representation allows aggregation to be done at the feature level, where variations in spatial patterns are handled more naturally. After the latent vectors are combined—often through a simple mean or another statistical operation, the decoder can reconstruct an image that reflects the shared characteristics of the dataset [7]. Several studies have reported that this strategy preserves important EEG topographic features much better than pixel-wise averaging, which tends to blur or distort spatial information when subjects differ substantially. Overall, this generative approach provides a more reliable way of producing summary images, especially when the dataset contains heterogeneous spatial activation patterns.

The objective of this study is to implement a Deep Convolutional Autoencoder as a two-dimensional visualization method for EEG signals. This approach is further supported by using a dataset capturing adolescents' brain responses to addiction-related terminology. The present work extends earlier analyses conducted by Wijayanto et al [3], [8]. on the same dataset, which previously explored one-dimensional and two-dimensional EEG characteristics in adolescents exposed to

p-ISSN 2301-7988, e-ISSN 2581-0588
DOI : 10.32736/sisfokom.xx.xx,
Submitted : , Revised : , Accepted : , Published :

addiction-related cues. The dataset comprises respondents classified into normal and at-risk categories, with response variables represented by fast and slow patterns. By applying this deep learning–based generative framework, the study contributes methodological novelty in both EEG visualization and signal interpretation.

More specifically, this study contributes to the development of a Latent-Space Aggregation approach for representing the average patterns of brain activity. Through this method, the model can generate aggregated representations derived from the existing dataset. The proposed generative framework offers a potential solution for estimating group-level brain activity in both normal and at-risk respondent categories, thereby revealing distinctions in activation patterns associated with fast and slow responses. The resulting visualizations also provide empirical support for hypotheses regarding how normal and at-risk adolescents cognitively respond to addiction-related terminology. In addition, this work introduces a form of methodological and thematic novelty within EEG research in Indonesia, particularly in the context of addiction terminology and adolescent neurocognitive responses.

II. METHODS

A. Datasets and Distribution

This study utilizes a dataset obtained from the Telkom University Dataverse (https://doi.org/10.34820/FK2/GW8JIV) [8]. The dataset contains both one-dimensional and two-dimensional EEG recordings capturing neural responses to addiction-related terminology. The stimuli presented during EEG acquisition was based on the Go/No-Go Association Task (GNAT). The dataset includes recordings from twelve adolescent participants, categorized into normal and at-risk groups. The primary focus of this research is the analysis of the two-dimensional EEG representations, from which the model generates average responses for both fast and slow conditions across the two respondent categories. This approach aims to provide a clearer depiction of group-level neural activation patterns associated with differing response speeds.

The total dataset used in this study consists of 812 topoplots images. Each respondent's data is categorized into fast and slow responses. The fast category corresponds to reaction times between 0 s and 0.5 s after stimulus onset, while the slow category represents responses occurring between 0.5 s and 1 s. The respondent groups are divided into two categories. The normal group contributes 492 images, comprising 260 fast responses and 232 slow responses. Meanwhile, the at-risk group contributes 320 images, consisting of 153 fast responses and 167 slow responses.

B. Autoencoder Architecture for Latent Space Aggregation

In designing the system, this study employs a Deep Convolutional Autoencoder (CAE). A CAE is an unsupervised learning architecture developed for training on high-dimensional data such as images. Unlike conventional autoencoders that rely solely on fully connected layers, a CAE incorporates convolutional operations to preserve the structural integrity of the input data [9]. This characteristic is essential in the context of EEG topoplots, where neighboring electrodes exhibit strong spatial correlations that must be retained. Structurally, the architecture consists of two symmetrical networks: an encoder pathway that functions as a feature extractor, and a decoder pathway responsible for reconstructing the input topoplots images.

The encoding process represents the input topoplots and transforms it through a series of convolutional operations. Each convolutional layer is computed using the following equation:

$$h_k = \sigma(W_k * h_{k-1} + b_k) \quad (1)$$

where * denotes the convolution operator W_k is the learnable kernel matrix, b_k is the bias term, and h_{k-1} is the input feature map [10], [11]. To reduce the spatial dimensions and achieve translational invariance, a Max-Pooling operation is applied after each convolutional block. This operation retains the maximum value within each patch, progressively reducing the input resolution from 128 x 128 to an abstract 16 x 16. feature representation.

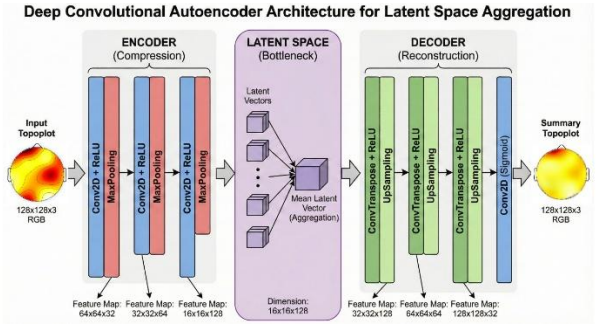

Figure 1. Schematic diagram of the proposed latent space aggregation framework.

The contribution of this study lies in the aggregation method performed within the latent space, as illustrated in the middle block of Figure 1. Unlike conventional approaches that compute the average directly from high-dimensional pixel values, the proposed method calculates the average from compressed feature representations. This latent-space averaging enables a more meaningful and compact characterization of EEG topoplots patterns, capturing essential structure while reducing noise and redundancy. High-dimensional pixel data are susceptible to biased artifacts. Therefore, a compression step is applied to remove such distortions before any averaging is performed at the pixel level.

Instead of computing the average across all individual samples, the averaging process is performed on input topoplots groups that have already been mapped into specific categories for example, the *at-risk–fast* group. The mean vector is then computed using the following equation:

$$z_{avg} = \frac{1}{N}\sum_{i=1}^{N} z_i \quad (2)$$

Where N denotes the total number of samples within the corresponding category, and z_{avg} represents the averaged latent vector computed for that respondent group [12], [13]. Once this latent average vector is obtained, it is then passed through the decoder to generate a reconstructed topoplots image. This technique preserves the sharp gradient characteristics embedded in the averaged latent representation, allowing the

p-ISSN 2301-7988, e-ISSN 2581-0588
DOI : 10.32736/sisfokom.xx.xx, Copyright ©2020
Submitted : , Revised : , Accepted : , Published :

resulting visualization to retain meaningful structural patterns.

III. Results and Discussion

A. Normal – Fast Category Respondents

Within the Normal category, the dataset comprises a total of 492 topoplots. These images were stratified based on reaction latencies recorded during the GNAT assessment, yielding 260 instances in the 'fast' category (reaction time < 0.5 s) and 232 in the 'slow' category (reaction time > 0.5 s). This segmentation is supported by prior literature suggesting that rapid responses particularly those under 250 ms are indicative of 'honest' or instinctive processing [14]. Consequently, the application of GNAT provides an optimal framework for isolating authentic neural responses within the analysis.

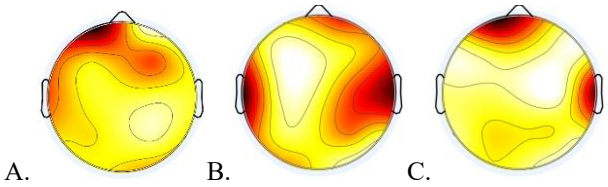

Figure 2. Examples of normal category in fast responses

Figure 2 visualizes the raw topoplots, exposing a marked inconsistency in how different subjects respond. The focal points of neural activity shift unpredictably ranging from localized left frontal activation in Respondent A, to bilateral temporal patterns in Respondent B, and a more diffuse frontal-temporal engagement in Respondent C. These examples illustrate that sharp activation peaks are not a constant feature in raw data. Furthermore, a dark baseline artifact dominates the background of these images. To prevent this non-informative noise from distorting the final aggregate, it must be suppressed before the averaging stage begins.

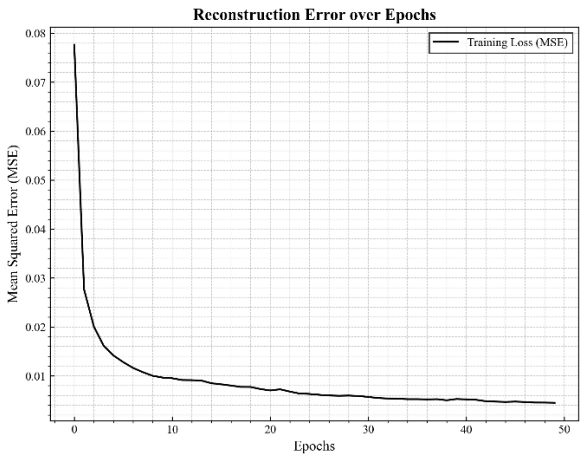

Figure 3. Reconstruction models error over epoch for normal-fast

To achieve high-fidelity image reconstruction, the model relies on the encoder's ability to map input data into a compressed latent representation. The training stability of this process is plotted in Figure 3, which tracks the error reduction trajectory over time. By the 50th epoch, the model converged successfully, driving the loss value down to below 0.01. This low-error state indicates that the network has effectively learned to isolate meaningful neural features from background noise. Consequently, we applied these trained parameters to the raw dataset to suppress the non-informative dark baseline. The practical impact of this denoising step which clarifies the active neural regions is visually demonstrated across Figures 4, 5, and 6.

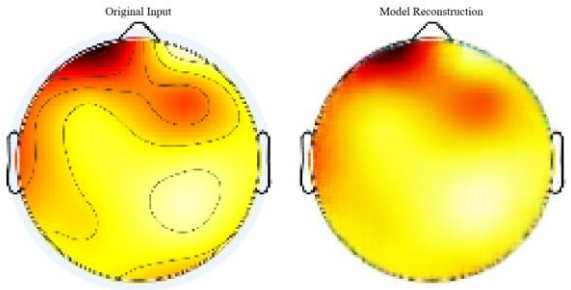

Figure 4. Reconstructed EEG topoplots output for respondent A after baseline removal

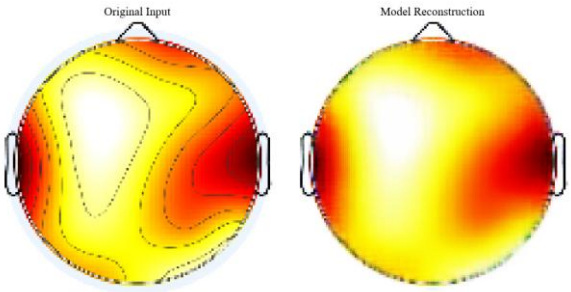

Figure 5. Reconstructed EEG topoplots output for respondent B after baseline removal

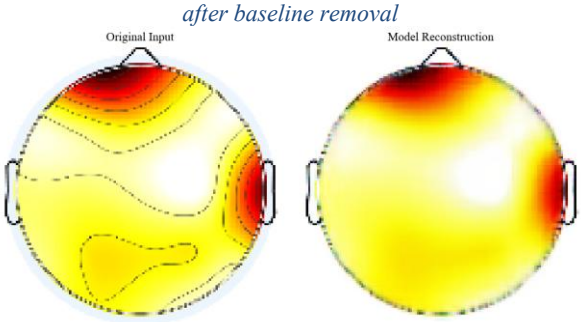

Figure 6. Reconstructed EEG topoplots output for respondent C after baseline removal.

The efficacy of the training process in eliminating baseline artifacts is visually demonstrated in Figures 4 through 6. As observed in these reconstructions, the model successfully isolates regions of genuine neural activity, effectively stripping away the dark background noise. Subsequently, these cleaned topoplots were subjected to an aggregation process. Specifically, for the 'Fast' response category, the averaging was performed not on raw pixels, but within the latent space representation to capture the shared structural features. The final aggregated output resulting from this method is presented in Figure 7.

p-ISSN 2301-7988, e-ISSN 2581-0588
DOI : 10.32736/sisfokom.xx.xx, Copyright ©2020
Submitted : , Revised : , Accepted : , Published :

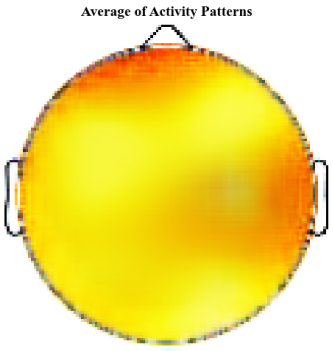

Figure 7. Average of activity patterns in normal-fast category respondent

As shown in Figure 7, the averaged results for the Normal-Fast category display a relatively diffuse neural signal. The activity does not cluster in a single point but spreads across the map in a gradient of yellow and orange. Deep orange tones, representing the highest intensity, dominate the frontal lobe, with moderate activation extending into the temporal sections. This heavy reliance on the frontal cortex implies a state of high focus and readiness to respond [15]. Such a configuration is unsurprising, as the interplay between frontal and temporal networks is a well-documented mechanism in cognitive response tasks [16], [17].

B. Normal – Slow Category Respondents

For the Normal respondents exhibiting slower reaction times (Normal-Slow), the dataset comprises 232 topoplots. This group was processed using the identical generative framework applied to the Fast category to ensure methodological consistency. To capture the diversity of the subjects within this subset, specific samples were selected from the total pool for comparative analysis. These representative instances, which illustrate the varying activation patterns, are displayed in Figure 8.

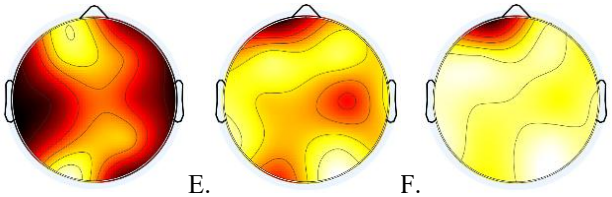

Figure 8. Examples of normal category in slow responses

A closer inspection of the Normal-Slow dataset reveals a marked increase in signal heterogeneity. As illustrated by the three sample variations, neural activity becomes far less uniform when respondents require more time to process addiction-related terminology. It appears that this extended processing window introduces a higher degree of individual variability in how the brain engages with the stimuli, resulting in divergent patterns. Despite this complexity, we proceeded with the training phase using the same autoencoder configuration applied to the Normal-Fast group. The model's performance in learning these diverse features is tracked in the training loss graph below.

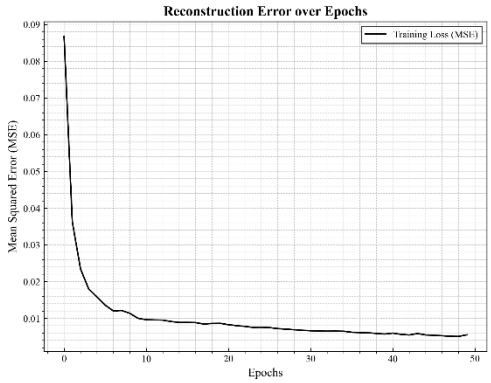

Figure 9. Reconstruction models error over epoch for normal-slow

The training progression, as plotted in Figure 9, demonstrates a consistent downward trajectory in Mean Squared Error (MSE) across all epochs. By the 50th iteration, the model achieved convergence, driving the error rate down to below 0.01. Interestingly, despite the higher variability inherent in this dataset, the loss pattern closely mirrors the stability observed in the Normal-Fast category. This suggests that the autoencoder is robust enough to handle the irregular patterns of slow responders without overfitting. The resulting generative outputs for the Normal-Slow group are presented below.

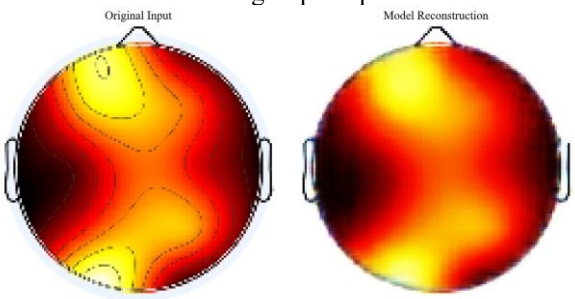

Figure 10. Reconstructed EEG topoplots output for respondent D after baseline removal

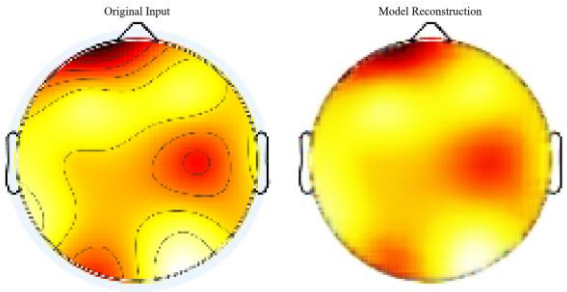

Figure 11. Reconstructed EEG topoplots output for respondent E after baseline removal

p-ISSN 2301-7988, e-ISSN 2581-0588
DOI : 10.32736/sisfokom.xx.xx, Copyright ©2020
Submitted : , Revised : , Accepted : , Published :

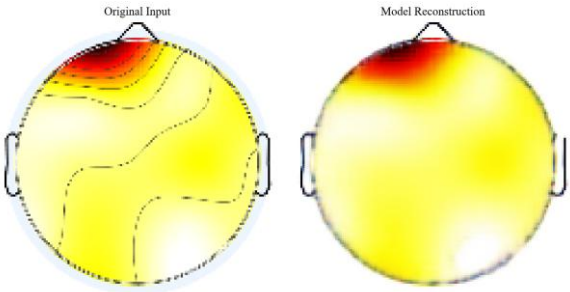

Figure 12. Reconstructed EEG topoplots output for respondent F after baseline removal

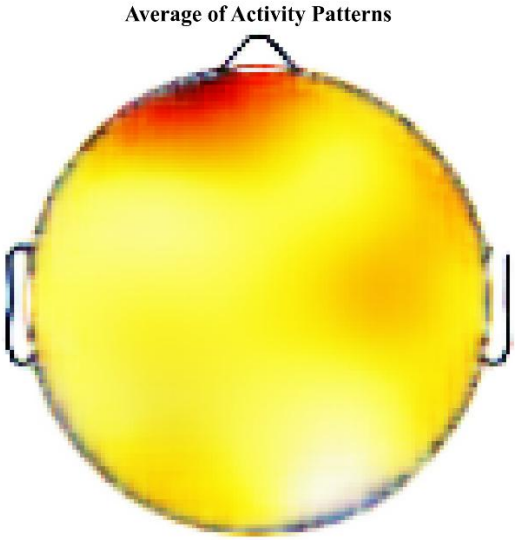

Figure 13. Average of activity patterns in normal-slow category respondent

The averaged topography in Figure 13 reveals a starkly concentrated activation pattern. Unlike the diffuse signals seen in other categories, the neural intensity here is almost exclusively confined to the frontal lobe, while the surrounding regions remain largely quiescent. This pronounced frontal dominance aligns well with established neuroscience literature, which identifies the prefrontal cortex as the central hub for executive functions, working memory, and complex decision-making [18]. The specific context of a 'slow' response offers a compelling interpretation for this localized intensity: it likely represents a cognitive bottleneck where the brain is heavily engaged in deliberating the stimulus. Rather than an immediate impulsive reaction, the high frontal load suggests the subject is actively recruiting executive resources to weigh the options before committing to a correct response.

C. At Risk – Fast Category Respondents

The analytical scope is next extended to the 'At-Risk' cohort, specifically focusing on the subset of respondents exhibiting rapid reaction times. This category, designated as 'At-Risk Fast', consists of a total of 153 EEG topoplot images. In alignment with the protocol established for the Normal group, several raw samples were extracted for preliminary visual inspection and are presented in Figure 14. These representative examples are essential for characterizing the baseline signal patterns, highlighting the inherent spatial variability in the data before the application of any generative processing or noise suppression techniques.

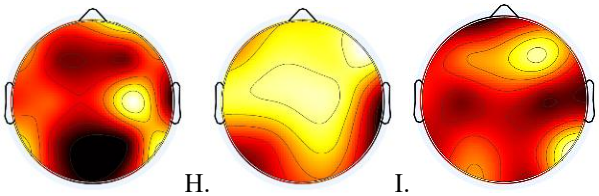

Figure 14. Examples of at-risk category in fast responses

A visual comparison reveals that the neural patterns within the At-Risk Fast category are significantly more chaotic and intensive than those observed in the Normal group. Unlike the focused activity seen previously, the three representative samples here exhibit a pervasive intensity, resulting in topoplots with a noticeably darker overall hue compared to both the Normal-Fast and Normal-Slow datasets. This widespread saturation suggests a heightened state of baseline neural arousal or noise. To address this complexity, the data was subjected to the autoencoder training pipeline. The quantitative performance of this training—specifically its ability to learn these dense features—is evaluated in the loss trajectory graph presented below.

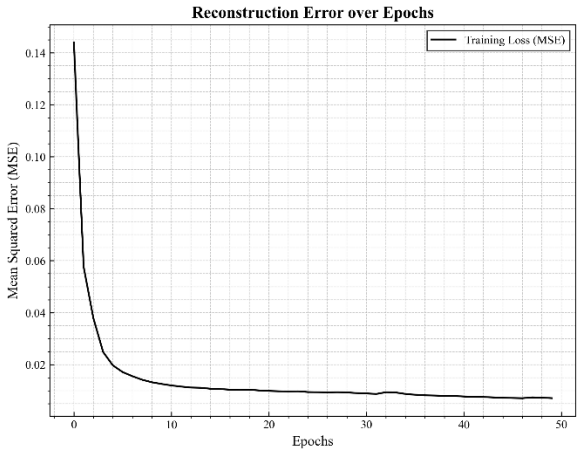

Figure 15. Reconstruction models error over epoch for at-risk fast

The loss trajectory plotted in Figure 15 reveals a consistent minimization of the Mean Squared Error (MSE). By the final epochs, the curve settles below the 0.01 threshold, marking a clear point of convergence. This result is particularly promising given the input's complexity; it confirms that the autoencoder is not merely memorizing noise but effectively disentangling the underlying structure from the chaotic 'Risk-Fast' signals. To validate this performance beyond numerical metrics, the trained model was subsequently engaged to reconstruct the three representative samples selected earlier. This step aimed to

p-ISSN 2301-7988, e-ISSN 2581-0588
DOI : 10.32736/sisfokom.xx.xx, Copyright ©2020
Submitted : , Revised : , Accepted : , Published :

visually assess the model's efficacy in stripping away the dominant baseline artifacts while retaining the integrity of the signal patterns, as illustrated in the resulting images below.

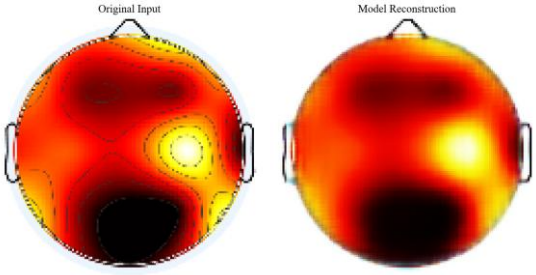

Figure 16. Reconstructed EEG topoplots output for respondent G after baseline removal

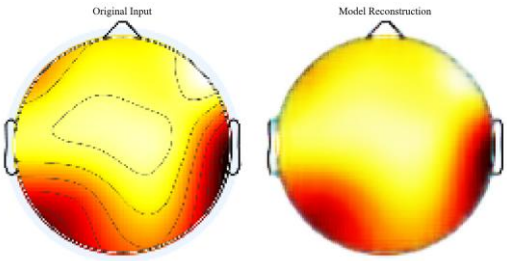

Figure 17. Reconstructed EEG topoplots output for respondent H after baseline removal

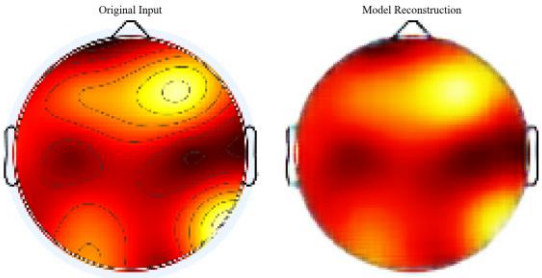

Figure 18. Reconstructed EEG topoplots output for respondent I after baseline removal

The reconstructive capabilities of the autoencoder are visualized in Figure 16 to Figure 18. Mirroring the efficacy observed in the Normal category, the model successfully filters out the baseline artifacts, ensuring that the output images strictly emphasize regions of potent neural activity while effectively silencing the background noise. Following this purification, the dataset undergoes the aggregation phase. Instead of relying on raw pixel averaging, we leverage a latent space approach to compute the mean representations, which yields a more comprehensive and structurally accurate visualization. The final synthesized pattern derived from this Risk-Fast cohort is presented in Figure 13.

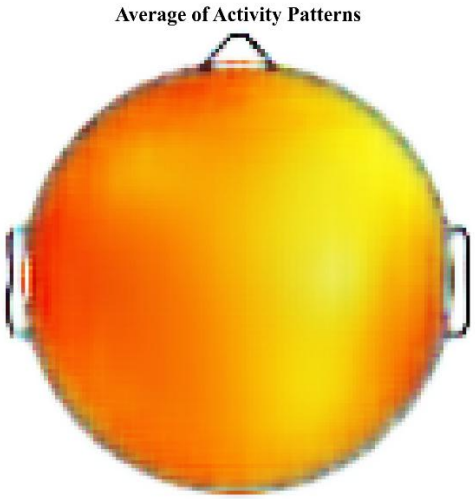

Figure 19. Average of activity patterns in at-risk fast category respondent

The averaged topography depicted in Figure 13 exposes a compelling neurophysiological anomaly: activity is not localized but is instead dispersed diffusely across the entire cortical surface. This pattern of excessive global activation—often referred to as cortical hyper-arousal—strongly suggests that the neural response is being modulated by intense emotional engagement rather than pure cognitive processing. Such findings resonate with the 'neural inefficiency' hypothesis in neuroscience, which posits that individuals with compromised impulse control or high anxiety must recruit significantly larger neural networks to achieve the same cognitive outcome as neurotypical peers [19]. In the context of this study, the presence of addiction-related terminology appears to trigger a reactive, emotionally charged state. Consequently, the rapid reaction times observed in this group should not be mistaken for cognitive efficiency; rather, they are likely driven by impulsivity [20], [21]. This visualization provides empirical evidence that At-Risk respondents are operating under a considerably heavier cognitive and emotional burden during the assessment.

D. At Risk – Slow Category Respondents

The remaining dataset focuses on 'At-Risk' respondents with delayed reaction times, a subset consisting of 167 topoplot images. Before attempting any reconstruction, it is critical to visually audit the raw inputs to grasp their irregularity. Figure 14 captures this baseline state. These samples expose the volatile nature of the signals in this group, offering a clear view of the chaotic fluctuations and high noise levels that the model is tasked with resolving.

p-ISSN 2301-7988, e-ISSN 2581-0588
DOI : 10.32736/sisfokom.xx.xx, Copyright ©2020
Submitted : , Revised : , Accepted : , Published :

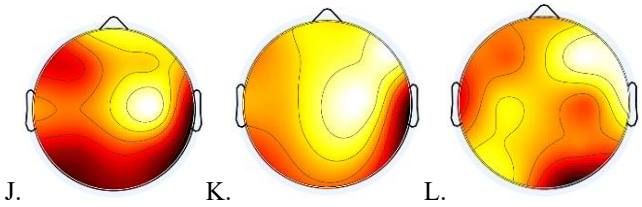

Figure 20. Examples of At-Risk category in slow responses

Visual inspection of Figure 14 uncovers a signal landscape defined by complex fluctuations and a predominantly dark intensity. However, a crucial distinction emerges when compared to the At-Risk Fast category: while the Fast group showed a uniform, global saturation, the Slow group exhibits a far more erratic spatial distribution. The patterns here are not consistent; instead, they display irregular variations in intensity across different respondents, although the overall signal amplitude remains noticeably higher (darker) than that of the Normal categories. Given this spatial incoherence, the subsequent model training phase was critical to suppress the noise and reconstruct the underlying topology. The quantitative performance of this process is tracked in the loss evaluation graph below.

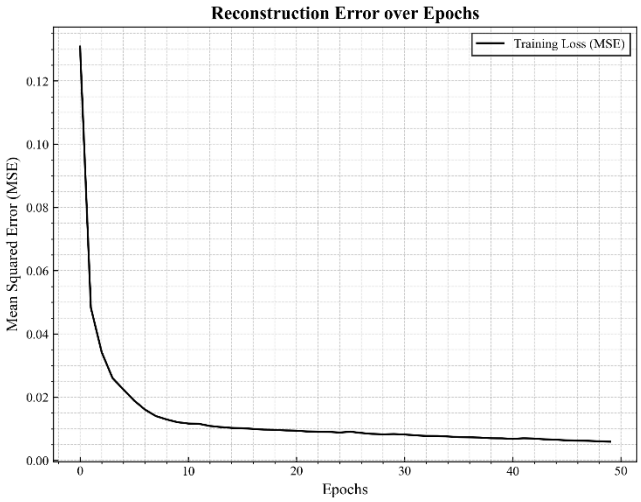

Figure 21. Reconstruction models error over epoch for Normal-Fast

The training metrics indicate that the loss function plateaued just above the 0.01 threshold (MSE > 0.01), preventing the deep convergence seen in the other groups. This slightly elevated error rate is indicative of the dataset's intrinsic heterogeneity; it reflects the unstable neural fluctuations that occur as 'Risk-Slow' respondents struggle to process the stimuli over a longer duration. Notwithstanding this statistical deviation, the qualitative results in Figure 21 demonstrate that the model remains highly effective. It successfully strips away the baseline artifacts, ensuring that the primary activity zones are clearly delineated from the background noise. With the signal thus purified, we proceeded to average the topoplots to map the group's collective cognitive focus. The resulting spatial distribution is visualized in Figure 22 to Figure 24.

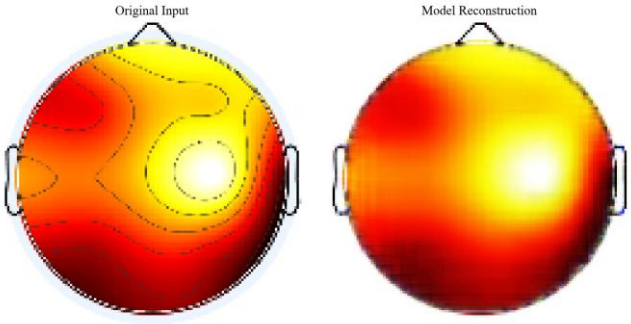

Figure 22. Reconstructed EEG topoplots output for respondent J after baseline removal

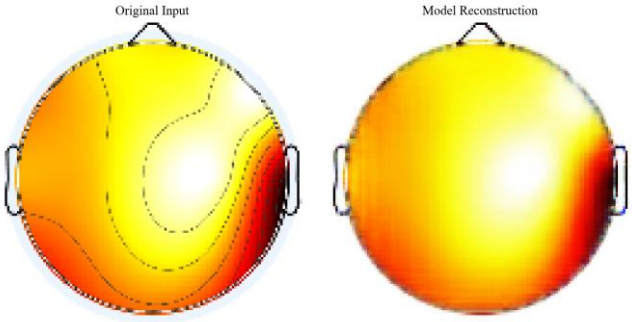

Figure 23. Reconstructed EEG topoplots output for respondent K after baseline removal

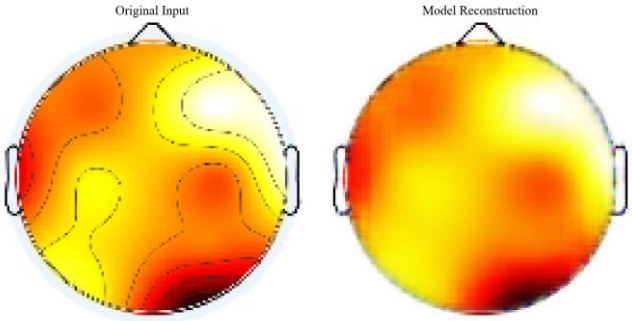

Figure 24. Reconstructed EEG topoplots output for respondent L after baseline removal.

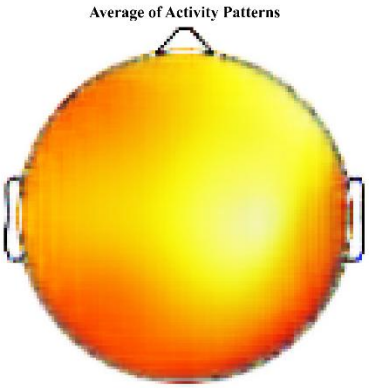

Figure 25. Average of activity patterns in at-risk slow category respondent

p-ISSN 2301-7988, e-ISSN 2581-0588
DOI : 10.32736/sisfokom.xx.xx, Copyright ©2020
Submitted : , Revised : , Accepted : , Published :

The averaged topography unveils a pronounced asymmetry in neural distribution. Activity is heavily concentrated in the posterior regions—specifically the Occipital and Temporal lobes—standing in stark contrast to the minimal engagement observed in the Frontal area. This pattern provides neurophysiological evidence supporting the 'Attentional Bias' framework often cited in addiction pathology. The heightened Occipital intensity suggests that respondents are visually fixated on the addiction-related cues, while the concurrent Temporal activation indicates the automatic retrieval of semantic or episodic memories associated with substance use [22]. Consequently, delayed reaction times can be interpreted as a failure of executive control: attentional resources are being disproportionately allocated to visual processing and memory recall, creating a bottleneck that hinders the Frontal lobe from executing a timely decision. Furthermore, this reduced frontal engagement aligns with existing studies showing that narcotic usage compromises the functional integrity of the prefrontal cortex [23].

IV. CONCLUSION

The comparative analysis conducted across the respondent categories elucidates that reaction time—whether fast or slow—is not merely a temporal metric but a reflection of distinct underlying neural strategies. The study successfully mapped these differences, revealing that 'Fast' responses in risk groups are driven by impulsive hyper-arousal, whereas 'Slow' responses are characterized by cognitive hesitation and scattered spatial attention. From a methodological standpoint, the implementation of the Autoencoder architecture emerged as a pivotal advancement for EEG topography analysis. Unlike traditional filtering methods which often degrade signal integrity, the Autoencoder leverages latent space representations to intelligently distinguish between genuine neural activity and baseline artifacts [24].

This generative approach proves to be highly effective in "masking" the baseline, thereby producing reconstructed topoplots that are both structurally complete and free from noise. By synthesizing clean data from complex, noisy inputs, this model offers a robust solution for the challenges of signal averaging in neuroinformatics [25]. Consequently, this research validates the Autoencoder not only as a tool for noise reduction but as a comprehensive framework for generative image processing, capable of uncovering subtle neural patterns that are otherwise obscured in raw EEG datasets.

The heterogeneity observed in the results, particularly within the 'At-Risk' cohorts, opens fertile ground for novel investigative pathways. The current study highlights that neural responses to addiction cues are highly individualized; thus, future research should aim to decode this variability using more sophisticated architectures. There is a compelling opportunity to extend this work by integrating Variational Autoencoders (VAEs) or Generative Adversarial Networks (GANs) to model the probability distribution of these diverse responses more precisely. Furthermore, incorporating Explainable AI (XAI) techniques would be a critical next step to interpret why the model focuses on specific cortical areas, bridging the gap between "black box" deep learning and clinical interpretability in addiction psychiatry. Longitudinal studies could also be employed to track how these topographical patterns evolve over time, offering potential biomarkers for monitoring rehabilitation progress.

ACKNOWLEDGMENT

This research was conducted with funding from a competitive postgraduate research grant v.

REFERENCES

[1] G. Placidi, L. Cinque, and M. Polsinelli, "Convolutional Neural Networks for Automatic Detection of Artifacts from Independent Components Represented in Scalp Topographies of EEG Signals," Sep. 2020, doi: 10.1016/j.compbiomed.2021.104347.

[2] V. Janiukstyte *et al.*, "Normative brain mapping using scalp EEG and potential clinical application," *Sci. Rep.*, vol. 13, no. 1, Dec. 2023, doi: 10.1038/s41598-023-39700-7.

[3] I. Wijayanto *et al.*, "Unlocking Early Detection and Intervention Potential: Analyzing Visual Evoked Potentials in Adolescents/ Teenagers with Narcotics Abuse Tendencies from the TelUnisba Neuropsychology Electroencephalograph Dataset," *J. Electron. Electromed. Eng. Med. Informatics*, vol. 6, no. 4, pp. 445–458, Oct. 2024, doi: 10.35882/jeeemi.v6i4.476.

[4] R. A. Clark, N. Nikolova, W. J. McGeown, and M. Macdonald, "Eigenvector alignment: Assessing functional network changes in amnestic mild cognitive impairment and Alzheimer's disease," *PLoS One*, vol. 15, no. 8 August, Aug. 2020, doi: 10.1371/journal.pone.0231294.

[5] T. Wen and Z. Zhang, "Deep Convolution Neural Network and Autoencoders-Based Unsupervised Feature Learning of EEG Signals," *IEEE Access*, vol. 6, pp. 25399–25410, May 2018, doi: 10.1109/ACCESS.2018.2833746.

[6] M. Q. Pérez, S. L. Bernal, E. H. Prat, L. M. Del Campo, L. F. Maimó, and A. H. Celdrán, "EEG channel reconstruction using convolutional neural networks in limited BCIs: A proposed method for neuromarketing applications," *Appl. Soft Comput.*, vol. 181, Sep. 2025, doi: 10.1016/j.asoc.2025.113455.

[7] T. Hoffmann, "Latent space approaches to aggregate network data," Mar. 2023, [Online]. Available: http://arxiv.org/abs/2303.08338

[8] I. Wijayanto, "TelUnisba Neuropsychology EEG Dataset (TUNDA)," 2024, *Telkom University Dataverse*. doi: 10.34820/FK2/GW8JIV.

[9] J. Masci, U. Meier, D. Cireşan, and J. Schmidhuber, "Stacked convolutional auto-encoders for hierarchical feature extraction," *Lect. Notes Comput. Sci. (including Subser. Lect. Notes Artif. Intell. Lect. Notes Bioinformatics)*, vol. 6791 LNCS, no. PART 1, pp. 52–59, 2011, doi: 10.1007/978-3-642-21735-7_7.

[10] R. Yamashita, M. Nishio, R. K. G. Do, and K. Togashi, "Convolutional neural networks: an overview and application in radiology," *Insights Imaging*, vol. 9, no. 4, pp. 611–629, 2018, doi: 10.1007/s13244-018-0639-9.

[11] S. Albawi, T. A. M. Mohammed, and S. Alzawi, "Understanding of a Convolutional Neural Network," *Icet2017*, pp. 1–6, 2017, doi: 10.1109/ICEngTechnol.2017.8308186.

[12] Y. Bengio, A. Courville, and P. Vincent, "Representation learning: A review and new perspectives," *IEEE Trans. Pattern Anal. Mach. Intell.*, vol. 35, no. 8, pp. 1798–1828, 2013, doi: 10.1109/TPAMI.2013.50.

[13] D. Berthelot, I. Goodfellow, C. Raffel, and A. Roy, "Understanding and improving interpolation in autoencoders via an adversarial regularizer," *7th Int. Conf. Learn. Represent. ICLR 2019*, 2019, doi: 10.48550/arXiv.1807.07543.

[14] E. M. Templeton, L. J. Chang, E. A. Reynolds, and M. D. Cone, "Fast response times signal social connection in conversation," vol. 119, no. 4, 2022, doi: 10.1073/pnas.2116915119/-

p-ISSN 2301-7988, e-ISSN 2581-0588
DOI : 10.32736/sisfokom.xx.xx, Copyright ©2020
Submitted : , Revised : , Accepted : , Published :

/DCSupplemental.Published.

[15] T. Emsawas, T. Kimura, S. Ogura, H. Morita, and E. Abdullajon, "Identifying english proficiency by frontal theta activity during english learning," *Discov. Educ.*, 2025, doi: 10.1007/s44217-025-00517-3.

[16] A. Valentin, R. Selway, G. Alarco, M. E. Lacruz, and J. J. Garcı, "Frontal and temporal functional connections of the living human brain," vol. 26, no. March, pp. 1357–1370, 2007, doi: 10.1111/j.1460-9568.2007.05730.x.

[17] M. Kotas, M. Piela, and S. Contreras-Ortiz, "Modified Spatio-Temporal Matched Filtering for Brain Responses Classification," *IEEE Trans. Human-Machine Syst.*, vol. 52, pp. 1–10, Jan. 2022, doi: 10.1109/THMS.2022.3168421.

[18] X. Liang, F. Xiao, Y. Lei, H. Li, and Q. Chen, "N400/frontal negativity reveals the controlled processes of taxonomic and thematic relationships in semantic priming for artifacts," *Psychophysiology*, vol. 57, no. 2, Feb. 2020, doi: 10.1111/psyp.13486.

[19] A. C. Neubauer and A. Fink, "Neuroscience and Biobehavioral Reviews Intelligence and neural efficiency," vol. 33, pp. 1004–1023, 2009, doi: 10.1016/j.neubiorev.2009.04.001.

[20] J. Zhang, L. Yang, Y. Zhang, H. Su, Y. Zhang, and Y. Yang, "Updating Emotional Stimuli in Heroin Abstainers' Working Memory: An Event-Related Potential Investigation," *Subst. Use Misuse*, vol. 56, no. 6, pp. 801–807, 2021, doi: 10.1080/10826084.2021.1899223.

[21] G. F. Koob and N. D. Volkow, "Neurobiology of addiction : a neurocircuitry analysis," *The Lancet Psychiatry*, vol. 3, no. 8, pp. 760–773, 2016, doi: 10.1016/S2215-0366(16)00104-8.

[22] Y. Yalachkov, J. Kaiser, and M. J. Naumer, "Sensory and motor aspects of addiction," vol. 207, pp. 215–222, 2010, doi: 10.1016/j.bbr.2009.09.015.

[23] A. O. Ceceli and C. W. Bradberry, "The neurobiology of drug addiction : cross-species insights into the dysfunction and recovery of the prefrontal cortex," no. August, 2021, doi: 10.1038/s41386-021-01153-9.

[24] T. Zhao *et al.*, "NeuroImage VAEEG : Variational auto-encoder for extracting EEG representation," *Neuroimage*, vol. 304, no. July, p. 120946, 2024, doi: 10.1016/j.neuroimage.2024.120946.

[25] M. Y. Sikkandar *et al.*, "Optimization Driven Variational Autoencoder GAN for Artifact Reduction in EEG Signals for Improved Neurological Disorder and Disability Assessment," no. 1, pp. 10–14, 2025, doi: 10.2478/msr-2025-0002.

p-ISSN 2301-7988, e-ISSN 2581-0588
DOI : 10.32736/sisfokom.xx.xx, Copyright ©2020
Submitted : , Revised : , Accepted : , Published :